Title

Targeted therapy with MXD3 siRNA, anti-CD22 antibody and nanoparticles for precursor B-cell acute lymphoblastic leukaemia

Journal

British Journal of Haematology, 167(4)

ISSN

0007-1048

Authors

Satake, Noriko
Duong, Connie
Chen, Cathy
et al.

Publication Date

2014-11-01

DOI

10.1111/bjh.13066

Peer reviewed

Published in final edited form as:
Br J Haematol. 2014 November ; 167(4): 487–499. doi:10.1111/bjh.13066.

Targeted therapy with MXD3 siRNA, anti-CD22 antibody and nanoparticles for precursor B-cell acute lymphoblastic leukaemia

Noriko Satake[*,1,2], **Connie Duong**[*,1,2], **Cathy Chen**[1,2], **Gustavo A. Barisone**[3], **Elva Diaz**[3], **Joseph Tuscano**[4], **David M. Rocke**[5], **Jan Nolta**[2], and **Nitin Nitin**[6]

[1]Department of Pediatrics, University of California Davis

[2]Stem Cell Program and Institute for Regenerative Cures, University of California Davis

[3]Department of Pharmacology, University of California Davis

[4]Department of Internal Medicine, University of California Davis

[5]Departments of Public Health Sciences and Biomedical Engineering, University of California Davis

[6]Departments of Food Science & Technology and Biological & Agricultural Engineering, University of California Davis

Summary

Conventional chemotherapy for precursor B-cell (preB) acute lymphoblastic leukaemia (ALL) has limitations that could be overcome by targeted therapy. Previously, we discovered a potential therapeutic molecular target, MDX3 (MAX dimerization protein 3), in preB ALL. In this study, we hypothesize that an effective siRNA therapy for preB ALL can be developed using antiCD22 antibody (αCD22 Ab) and nanoparticles. We composed nanocomplexes with super paramagnetic iron oxide nanoparticles (SPIO NPs), αCD22 Abs and MXD3 siRNA molecules based on physical interactions between the molecules. We demonstrated that the MXD3 siRNA-αCD22 Ab-SPIO NP complexes entered leukaemia cells and knocked down MXD3, leading the cells to undergo apoptosis and resulting in decreased live cell counts in the cell line Reh and in primary preB ALL samples *in vitro*. Furthermore, the cytotoxic effects of the MXD3 siRNA-αCD22 Ab-SPIO NP complexes were significantly enhanced by addition of the chemotherapy drugs vincristine or doxorubicin. We also ruled out potential cytotoxic effects of the MXD3 siRNA-αCD22 Ab-SPIO NP complexes on normal primary haematopoietic cells. Normal B cells were affected while CD34-positive haematopoietic stem cells and non-B cells were not. These data suggest that

Corresponding author: Noriko Satake, M.D., Section of Hematology/Oncology, Department of Pediatrics, University of California Davis, 2516 Stockton Blvd., Sacramento, CA 95817, Phone: 916-734-5387, FAX: 916-456-2236, noriko.satake@ucdmc.ucdavis.edu.
*These authors contributed equally to this work.

Authorship
N.S. and C.D. designed, performed research, analysed the data, and wrote the paper. All co-authors contributed essential reagents and wrote the paper. D.M.R. assisted with all the data analysis.

Conflict of Interest
The authors declare no conflict of interest.

MXD3 siRNA-αCD22 Ab-SPIO NP complexes have the potential to be a new targeted therapy for preB ALL.

Keywords

MXD3 siRNA; antiCD22 antibody; superparamagnetic iron oxide nanoparticle; precursor B-cell acute lymphoblastic leukaemia; RNA inhibition

Leukaemia is the most common malignancy in children, with precursor B-cell (preB) acute lymphoblastic leukaemia (ALL) being the most common type (Mullighan, 2012; Wiemels, 2012). Despite some progress, outcomes of certain subtypes of preB ALL still remain poor, with survival rates as low as 30% (Pui *et al.*, 2008). The outcome of ALL in adults, 70% of which is B-cell type ALL, is also poor with a survival rate of approximately 40% (Kato *et al.*, 2013). Unfortunately, there are no effective salvage treatments for those patients. In addition, many children who survive leukaemia suffer from “late effects,” which are serious life-long side effects from systemic chemo- and radiation therapy (Zerra *et al.*, 2013; Krishnan & Rajasekaran, 2014). These late effects include secondary malignancies and dysfunction of multiple organ systems (i.e., endocrine, skeletal, cardiovascular and nervous) and are usually irreversible. As the number of leukaemia survivors increases, the serious life-long late effects are a growing problem as more of these young children face far-reaching quality of life challenges.

To avoid the limitations and significant long-term side effects of current treatments, it is necessary to develop targeted therapies using new approaches. A few targeted therapies have been successfully used in clinic for different leukaemias, such as a BCR-ABL1 tyrosine kinase inhibitor in chronic myeloid leukaemia (and in BCR-ABL1 positive ALL) and all-*trans* retinoic acid in acute myeloid leukaemia (Hochhaus & Kantarjian., 2013; Sanz *et al.*, 2013). Furthermore, ongoing research has identified multiple molecular targets and therapeutic approaches in different types of cancers, including monoclonal antibodies with or without drug conjugates, tyrosine kinase targeting agents and inhibition of various pathways essential for cancer cells (Barth *et al.*, 2012; August *et al.*, 2013; Brown, 2013; Daver & O'Brien, 2013).

Previously we discovered that the MAX dimerization protein 3 (MXD3) transcription factor, a member of the MYC/MAX/MXD family of basic helix-loop-helix proteins, can be a therapeutic molecular target in preB ALL (unpublished observations). MXD3 has the potential to be a therapeutic target not only because it is highly expressed in preB ALL but also because its expression is generally limited to B cells, both normal and malignant (based on the current study and http://www.genecards.org/cgi-bin/carddisp.pl?gene=MXD3&search=a026324439964c3975c0e4c3ffa46513). Current chemotherapeutic drugs work through targets, such as dihydrofolate reductase or glucocorticoid receptor; however, these targets are not specific with expression in many tissue types and thus targeting them would result in considerably greater systemic toxicities. In a separate study, we also demonstrated the therapeutic efficacy of antiCD22 antibody-drug conjugates in preB ALL (Kato *et al.*, 2013). Here we report the development of a novel targeted therapy using

MXD3 siRNA, superparamagnetic iron oxide (SPIO) nanoparticles (NPs), and anti-CD22 antibodies (αCD22 Abs).

Materials and Methods

Reagents

The MXD3 siRNA sequence was 5'-AUGGACUAAAAGGACCCUUTT-3' (sense) and 5'-AAGGUCCUUUAGUCCAUTT-3' (antisense). The 3' end of the antisense strand was tagged with Alexa Fluor 488 (A488) (Qiagen, Valencia, CA). As a control, AllStars Negative siRNA was used, which has no known homology to mammalian genes and has minimal nonspecific effects (Qiagen, Valencia, CA). The 3’ end of the control RNA was also tagged with the A488.

Superparamagnetic iron oxide nanoparticles (SPIO NPs) with amphiphilic polymer and polyethylenimine (PEI) coating (iron core diameter: 15 nm) were purchased from Ocean Nanotech (San Diego, CA). Amine-modified SPIO NPs were fluorescently tagged with Alexa Fluor 532 (A532) succinimidyl ester (Life Technologies, Grand Island, NY). The surface of the NP was coated with fluorescein isothicyanate (FITC) conjugated anti-CD 22 antibody (αCD22 Ab) (BD Biosciences) to enable the NP complexes to target leukaemia cells.

Clinical-grade doxorubicin and vincristine (discarded after clinical use) were provided by University of California (UC) Davis Pharmacy.

Cells and cell cultures

Two human ALL cell lines were used in this study: Jurkat (T cell ALL), provided by the Kit Lam laboratory at UC Davis, and Reh (preB ALL), purchased from American Type Culture Collection (ATCC; Manassas, VA). Cells were maintained in 75 cm^2 plastic tissue culture-treated flasks (Corning Inc., Corning, NY) at 37 °C in a 5% CO_2 incubator. Both cell lines were grown in complete medium formulated with RPMI 1640 medium (Life Technologies, Grand Island, NY) supplemented with 10% heat-inactivated fetal bovine serum (Thermo Scientific, Pittsburgh, PA), 100 u/ml penicillin and 100 μg/ml streptomycin (Thermo Scientific, Pittsburgh, PA), 0.25% D-glucose (Sigma-Aldrich, St Louis, MO), 1 mM sodium pyruvate (Thermo Scientific, Pittsburgh, PA), and 10 mM HEPES buffer (Thermo Scientific, Pittsburgh, PA). Cells were manually washed and counted in phosphate-buffered saline (PBS; Thermo Scientific, Pittsburgh, PA) using trypan blue exclusion (0.04%, Sigma-Aldrich, St Louis, MO) and a haemocytometer. Cells were used within the first 25 passages and were maintained at their logarithmic phase of growth prior to each experiment.

Primary patient leukaemia samples were collected from patients with informed consent based on our institutionally approved Institutional Review Board (IRB) protocol and transplanted into female NOD/SCID/IL2Rg−/− (NSG) mice using our institutionally approved animal care protocol. As mice developed leukaemia, they were sacrificed and leukaemia cells were harvested from the leukaemia-infiltrated spleen and bone marrow for experiments. Human leukaemia cells were confirmed by flow cytometry using anti-HLA-

ABC Ab (Biolegends, San Diego, CA) and B-cell leukaemia panels, including anti-CD10, 19, 20 and 22 antibodies (BD Biosciences, San Diego, CA).

Normal blood cells were collected from anonymized discarded apheresis bags from healthy donors with IRB approval. B cells (lymphocytes) and CD34 positive (+) haematopoietic stem cells (HSCs) were isolated using magnetic beads (Miltenyi, San Diego, CA) and non-B cells were collected from the counterpart of B cell isolation. Cell purity of the isolated B cells and CD34+HSCs was confirmed by flow cytometry (FC500 Beckman Coulter) using anti-CD34 and anti-CD19 Ab, respectively. CD19-positive, CD20-negative immature B cells were collected by an Influx flow cytometer cell sorter (BD Biosciences, San Jose, CA).

siRNA nanoformulations

Fresh nanocomplexes were made for each experiment. SPIO NPs were briefly vortexed with an amine-reactive succinimidyl ester labelled with A532 and incubated in the dark at 4 °C for 3 h. The molar ratio of SPIO to succinimidyl ester was 1:1. After incubation, the labelled SPIOs were mixed with αCD22 Abs and either control siRNA or MXD3 siRNA in water. The siRNA molecules were adsorbed on the surface of the A532-labelled SPIO NPs based on electrostatic interactions between the negative backbone of siRNA molecules and the amine-modified SPIO NPs. The antibody molecules were also physically adsorbed onto the NP surface. The ratio of αCD22Ab:siRNA:SPIO NP by mass was 0.2 : 1 : 1 and by mole was 5 :264 : 1, respectively. Standard molecular weight for IgG Ab was used for αCD22 Ab and molecular weights for siRNA and SPIO NP were obtained from the manufacturer (Qiagen and Ocean Nanotech, respectively). The αCD22 Abs and siRNAs were simultaneously added to the labelled SPIO NPs by vortexing for 5 s. The complete nanocomplexes were then mixed with Opti-mem Reduced Serum Medium (Life Technologies, Grand Island, NY) and added to each well, resulting in a final volume of 2ml per well.

Characterization of the nanocomplexes was performed using diffraction light scattering (DLS) on a Zetasizer Nano ZS (Malvern, UK) in ultrapure water to measure the hydrodynamic diameter and zeta potential of the nanocomplexes. Briefly, 0.5 mg of SPIO NPs (without A532 labelling) was combined with siRNAs and αCD22 Abs as described above and diluted in 1 ml of water. Measurements were performed 3 times in succession. Zeta potentials were determined using the Smoluchowski model (Doane *et al.*, 2012).

To measure loading efficiency of siRNAs and αCD22 Abs on SPIO NPs, the mixed solution was centrifuged at 900 g for 4 min. The pelleted nanocomplexes and supernatant, which contained unbound siRNAs and/or αCD22 Abs, were collected separately. The amount of siRNA and αCD22 Ab present in the supernatant and in the pelleted nanocomplexes was quantified using fluorescence titration curves.

Cell viability following treatment with siRNA nanocomplexes and chemotherapy drugs

Reh cells were plated directly before treatment with siRNA nanocomplexes at 200,000 cells/1 ml Opti-mem/well in 6-well tissue culture-treated plates. Wells were prepared in triplicates for each treatment group and time point. The Reh cells were incubated with the siRNA nanocomplexes for 4 h at 37 °C in a 5% CO_2 incubator. After 4 h, intracellular

delivery of the siRNA nanocomplexes was assessed using an inverted fluorescent microscope (Nikon, Tokyo, Japan). Opti-mem media was then replaced with complete Reh media. Live cell counts were performed at 4, 8, 24, 48 and 72 h after siRNA nanocomplex treatment, and the cells were collected for MXD3 protein expression by immunocytochemistry. The entire experiment was repeated 3 times. To test chemotherapy drugs with siRNA nanocomplexes, doxorubicin or vincristine was added either at 4 or 24 hs after siRNA nanocomplex treatment, at a concentration corresponding to the 50% inhibitory concentration (IC50) of each drug for Reh cells, which had been determined by prior MTS (3-(4,5-dimethylthiazol-2-yl)-5-(3-carboxymethoxyphenyl)-2-(4-sulfophenyl)-2H-tetrazolium) assays. MTS assay was carried out for each drug 3 times and the average IC50 was calculated. The average IC50 for doxorubicin and vincristine was 2.56 ng/ml and 1.18 ng/ml, respectively.

Immunocytochemistry and fluorescent image intensity quantification

To evaluate MXD3 expression at the protein level in cells that were treated with siRNA nanocomplexes, cells were collected and fixed with 10% buffered formalin and mounted on slides for fluorescent immunocytochemistry. Slides were incubated with anti-MXD3 monoclonal mouse Ab (Antibodies, Inc., Davis, CA) overnight at 4 °C, then with a secondary goat anti-mouse Ab conjugated to A488 (Life Technologies, Grand Island, NY). DAPI (4',6-diamidino-2-phenylindole) was used for nuclei visualization (Life Technologies, Grand Island, NY).

Fluorescent image intensity for cells treated with siRNA nanocomplexes was quantified using ImageJ (National Institutes of Health, Bethesda, MD). Representative fluorescent images of cells from each treatment type on a given field were used to determine the average level of MXD3 expression by mean fluorescent intensity (MFI). MFI was calculated by manually forming a boundary around each cell and determining the average pixel intensity per cell. The background fluorescent signal was subtracted from the MFI of each cell to obtain the corrected MFI.

Apoptosis assay

Cell apoptosis in Reh cells treated with siRNA nanocomplexes was measured by flow cytometry using annexin V conjugated to allophycocyanin (APC; BD Biosciences, San Diego, CA). Briefly, Reh cells were treated with siRNA nanocomplexes (without A532 labelling) as described above and collected 2 and 4 h after treatment. Cells were washed, counted, and resuspended in binding buffer and stained with DAPI and annexin V according to the manufacturer's instructions. Samples were analysed by the Fortessa flow cytometer (BD Biosciences, San Diego, CA) and the data were analysed by FlowJo. The experiment was repeated.

Caspase activity in Reh cells treated with the siRNA nanocomplexes was measured using the Caspase 3/7 Glo kit (Promega, Madison, WI). Reh cells were treated with siRNA nanocomplexes as described above and collected 2 and 4 h after treatment. Cells were then washed, counted in triplicates, resuspended in 50 μl of PBS in each well. Each sample was mixed with 50 μl of Caspase 3/7 Glo reagent and incubated for 1 h according to the

manufacturer's instructions. The samples were analysed using a Centro LB 960 Microplate Luminometer (Berthold Technologies, Oakridge, TN). The experiment was repeated.

Statistical methods

Statistical analysis was performed on all experiments using standard linear models implemented in the R statistics package, version 3.0.2 (*R Foundation f*or *Statistical Computing*, Vienna, Austria). Multiple comparisons of means used the R package multcomp (Hothorn & Zeileis, 2008; Hothorn *et al.*, 2008) employing Tukey's studentized range statistics. A P value <0·05 was considered significant for all statistical calculations.

Results

Characterization of αCD22 Ab-siRNA-SPIO NPs

We investigated the use of MXD3 siRNA as a novel therapeutic for preB ALL. To increase efficient intracellular delivery of siRNA, we used SPIO NPs and also αCD22 Ab as a leukaemia-specific targeting agent. To demonstrate the proof of principle, the siRNAs were combined with SPIO NPs based on electrostatic interactions between the NPs and siRNA molecules. The αCD22 Abs were physically adsorbed onto the surface of NPs for specific targeting.

First we characterized the size and charge of the final nanocomplexes: siRNA-αCD22 Ab-SPIO NPs. In order to track the siRNA-αCD22 Ab-SPIO NPs, we first labelled the SPIO NPs with A532. The size of the SPIO NPs with A532 was 47.4 nm in diameter (polydispersity 0.213, average diameter from 3 repeated measurements). Once combined with siRNA and αCD22 Ab, the size of the siRNA-αCD22 Ab-SPIO NPs was 93.8 nm in diameter (polydispersity 0.125) (Figure 1). Surface charges of the SPIO NPs with A532 alone and the siRNA-αCD22 Ab-SPIO NPs were +65.3 mV and +46.6 mV, respectively (Figure 1).

Next we evaluated the loading efficiency of both siRNA and αCD22 Ab on the NPs. The results of fluorescence measurements showed highly efficient loading of siRNA-A488 on the NPs: 95.3% of the siRNAs were loaded when alone to the NPs and 100% were loaded with αCD22 Abs to the NPs. αCD22 Abs-APC was also loaded with high efficiency (89.9%) when loaded alone to the NPs, but 47.1% when loaded with siRNAs (Table I). These results confirm that our siRNA-αCD22 Ab-SPIO NP complexes have the appropriate size and charge to be used as therapeutics (Li *et al.*, 2013; van der Meel *et al.*, 2013).

Cell-targeted delivery of the nanocomplexes to preB ALL cells, but not T ALL cells

To evaluate cell-specific targeting properties of αCD22 Ab, we tested the siRNA-αCD22 Ab-SPIO NPs on Reh and Jurkat cells. Reh cells express CD22 whereas Jurkat cells do not (Kato *et al.*, 2013). When Reh and Jurkat cells were treated *in vitro* under the same conditions with the MXD3 or control siRNA-αCD22 Ab-SPIO NPs, only Reh cells showed uptake of the siRNA-αCD22 Ab-SPIO NPs (data not shown).

To determine the optimal amount of αCD22 Abs to load onto the SPIO NPs, we tested the MXD3 siRNA-SPIO NPs (1 μg of siRNAs and NPs) with 2, 0.2 and 0.02 μg of αCD22 Abs

and treated Reh cells *in vitro*. Efficiency in MXD3 knockdown by each αCD22 Ab amount was quantified by immunocytochemistry on the treated cells. Because the MXD3 knockdown effect had plateaued when increasing the αCD22 Abs load on the nanocomplexes, we chose the 0.2:1 ratio of αCD22 Ab:SPIO NPs.

Next we tested the MXD3 siRNA-SPIO NPs on the Reh cells with or without αCD22 Abs on the nanocomplexes (Figure 2A). After delivery of siRNA nanocomplexes, there was a trend towards higher MXD3 knockdown with αCD22 Abs than without αCD22 Abs (average knockdown 70% vs. 42%, not statistically significant) (Figure 2B). Therefore, the addition of αCD22 Abs to the nanocomplexes showed selective and more efficient delivery of siRNA to Reh cells.

Intracellular uptake, target-specific delivery of siRNA, and gene silencing effects

We next investigated *in vitro* therapeutic effects of the nanocomplexes MXD3 siRNA-αCD22 Ab-SPIO NPs in Reh cells. The fluorescent-labelled MXD3 or control siRNA-αCD22 Ab-SPIO NPs were observed inside Reh cells 4 h after a single treatment with the siRNA nanocomplexes (Figure 3A). Co-localization of the A488-conjugated siRNA (and possibly FITC-conjugated αCD22 Abs) and A532-conjugated SPIO NPs was observed inside the treated cells, indicating that the siRNA nanocomplexes entered the cells as a whole. Although the FITC-conjugated αCD22 Ab and A488-conjugated siRNA cannot be distinguished using fluorescent imaging, we have demonstrated that most of the fluorescent signal in the FITC channel is contributed by A488-conjugated siRNA, with minimal signal from FITC-conjugated αCD22 Ab due to the amount of each molecule on the NP surface and the difference in signal intensity between FITC and A488 (data not shown). The cells treated with the MXD3 siRNA nanocomplexes showed a 70.6% reduction in MXD3 protein expression 4 h after treatment (Figure 3B and C). MXD3 knockdown effects lasted until 72 h after treatment (data not shown). Cells that were treated under identical conditions with control siRNA nanocomplexes or untreated cells did not show knockdown in MXD3 protein expression (Figure 3B and C). Importantly, Reh cells treated with the MXD3 siRNA nanocomplexes showed significantly reduced live cell counts over 72 h after treatment (Figure 3D).

To determine the mechanism behind the reduced cell counts, we assessed cell death by two cell viability assays: annexin V and DAPI, and caspase activity assays. The cells treated with MXD3 siRNA nanocomplexes showed significantly increased annexin V- and DAPI-positive cells than untreated or control siRNA nanocomplex-treated cells both 2 and 4 h after a single treatment (Figure 4A and B). At 2 h after treatment, untreated or control siRNA nanocomplex-treated cells showed more live than dead cells (average percentages of live vs. dead cells: 74.0% vs. 10.4% and 65% vs. 14.0%, respectively) (Figure 4B). On the other hand, MXD3 siRNA nanocomplex-treated cells showed fewer live cells than dead cells (average percentages of live vs. dead cells: 22.1 % vs. 41.3%) (Figure 4B). At 4 h, the live and dead cell ratio remained similar in the untreated cells and control siRNA nanocomplex-treated cells (average percentages of live vs. dead cells: 76.8% vs. 11.6% and 70.8% vs. 11.4%, respectively); however, there were significantly more dead cells than live cells in the MXD3 siRNA nanocomplex-treated cells (average percentages of live vs. dead

cells: 20.8% vs. 61.2%) (Figure 4B). Cells were also analysed for caspase 3 and 7 activities 2 and 4 h after treatment. At 2 h after treatment, there was a significant increase in caspase activity in the MXD3 siRNA nanocomplex-treated cells compared to untreated cells. At 4 h, the MXD3 siRNA nanocomplex-treated cells had significantly higher levels of caspase activity than both untreated and control siRNA nanocomplex-treated cells (Figure 4C). These results indicate that MXD3 knockdown led the cells to apoptosis to some extent, and that the knockdown effects began as early as at 2 h after siRNA was introduced to the cells.

Treatment effects of the MXD3 siRNA-αCD22 Ab-SPIO NPs on primary cells

After studies with the Reh cell line, we determined the *in vitro* effects of the siRNA nanocomplexes on primary preB ALL cells and normal blood cells. We first determined the MXD3 protein expression levels in 10 different primary patient preB ALL samples, with Reh as a control for high MXD3 expression and CD34+HSCs as a negative control (Figure 5A). All of the tested samples showed similar MXD3 protein expression levels to Reh cells, and higher expression compared to CD34+HSCs. We treated four primary ALL samples (S82, 83, 86 and 89) with the siRNA nanocomplexes *in vitro* the same way as described above for the Reh cells. The results of sample 86 are shown in Figure 5B to D. The MXD3 siRNA nanocomplexes demonstrated efficient intracellular uptake and knockdown of MXD3 expression (72.6% reduction in MXD3 expression compared to untreated cells) in these primary leukaemia cells, similar to Reh cells (Figure 5B and C). None of the sample 86 cells proliferated *in vitro*, and the cells treated with the MXD3 siRNA nanocomplexes showed accelerated cell death over the 72 h of treatment (Figure 5D).

We next assessed the potential toxicities of the siRNA nanocomplexes on normal blood cells including B cells and CD34+HSCs. Isolated B cells, non-B cells and CD34+HSCs showed purity greater than 97% by flow cytometry (data not shown). B cells express CD22 (Kato *et al.*, 2013). We also confirmed that B cells express MXD3 protein at the level of 50% of Reh cells whereas non-B cells and CD34+HSCs express negligible MXD3 protein (Figure 6A). These cells were treated with the siRNA nanocomplexes the same way as described above for the Reh and primary ALL samples. As expected, B cells showed uptake of the siRNA nanocomplexes and reduced MXD3 protein expression similar to Reh when treated with the MXD3 siRNA nanocomplexes (Figure 6B and C). Less uptake was observed in non-B cells and CD34+HSCs (data not shown). Non-B cells and CD34+HSCs did not exhibit any significant difference in MXD3 protein expression between untreated, MXD3 and control siRNA nanocomplex-treated conditions (data not shown). The live cell count after the siRNA nanocomplex treatment showed significantly accelerated cell death in the MXD3 siRNA nanocomplex-treated cells compared to cells treated with control siRNA nanocomplexes or untreated cells (Figure 6D). In non-B cells and CD34+HSCs, there was significantly accelerated cell death in both the MXD3 or control siRNA nanocomplex-treated cells compared to untreated cells. However, between the two nanocomplex-treated groups (MXD3 or control siRNA) there was no significant difference in death rate, implying that the main cause of cell death was due to the toxicity of NPs (Figure 6D).

Additive effects between the siRNA-αCD22 Ab-SPIO NPs and doxorubicin or vincristine

To study the possible additive effects that the siRNA nanocomplexes may have when administered with common chemotherapy drugs currently used to treat ALL, we tested a combination regimen of doxorubicin or vincrinstine with the siRNA nanocomplexes in Reh cells *in vitro*. A single dose of doxorubicin or vincristine, at a dose equivalent to the 50% inhibitory concentration (IC50) of each drug for Reh cells, was added to Reh cells 4 h after treatment with the siRNA nanocomplexes. A combination therapy of the MXD3 siRNA nanocomplexes and either drug showed significantly higher cytotoxicity than monotherapy (MXD3 siRNA nanocomplexes or chemotherapy drug alone) (Figure 7). We also added the drugs 24 h after the siRNA nanocomplex treatment. However, the additive effects were not significant in this cohort. These results demonstrate the strong potential of using siRNA nanocomplexes as a part of current chemotherapy regimens for preB ALL treatment.

Discussion

An ideal cancer-targeted therapy must have both a cancer-specific target and a vehicle to deliver drugs to its target. It is particularly important to develop a therapy with less systemic side effects on growing children than current therapies. In this study, we have demonstrated that our novel siRNA nanocomplexes have several advantages as a potential targeted therapy for preB ALL.

First, *MXD3* RNA seems to be an ideal molecular target for preB ALL. In our previous study, we demonstrated that MXD3 is anti-apoptotic in preB ALL (unpublished observations). In this study, our results showed that significant knockdown of MXD3 protein was achieved within 2 h after a single treatment of the siRNA nanocomplexes, leading to an increase in apoptosis of leukaemia cells (Figure 4). While this modest increase was statistically significant (all p-values were < 0.05 in Figure 4B and C), it may not correlate with *in vivo* efficacy. It is, however, important to note that a single treatment led to significant MXD3 knockdown, cell death and decreased live cell counts or accelerated cell death in Reh or primary ALL cells, respectively. Dysregulation of apoptotic pathways is one of the mechanisms for treatment resistance in cancers (Kumar *et al.*, 2013; Ramsay & Rodriguez-Justo, 2013). Therefore, targeting MXD3 for restoration of apoptosis is a promising approach, particularly when it is combined with other drugs with different treatment mechanisms. Furthermore, our results suggest that the turnover time of MXD3 protein is very short. It is possible to enhance the cell apoptotic effects by multiple dosing of the siRNA nanocomplexes. Our results showed that not only is MXD3 protein highly expressed in preB ALL cells (Figure 5A), but also, among normal blood cells, B cells are the only cell lineage that expresses MXD3 protein, although its expression is less than half of that in preB ALL cells (Figure 6A). It is particularly important that our results showed CD34+HSCs do not express MXD3, as an ideal targeted therapy should avoid toxicities on HSCs. Data at Gene Cards (http://www.genecards.org/cgi-bin/carddisp.pl?gene=MXD3&search=a026324439964c3975c0e4c3ffa46513) show relatively low *MXD3* mRNA levels in normal human tissues and no MXD3 protein expression except in plasma. It is necessary to carefully evaluate potential toxicities and off-target effects of our MXD3

siRNA; however, because of the preferential expression in preB ALL cells, MXD3 is a potential therapeutic target.

Second, the addition of αCD22 Abs to our nanocomplexes is the key for achieving cell-specific targeting of preB ALL cells. Our previous study and others have shown that αCD22 Ab drug-conjugates offer promising new therapies for B-cell malignancies (Mussai *et al.*, 2010; Hoelzer, 2013; Kato *et al.*, 2013). High CD22 expression is known to be limited to normal and malignant B cells, including preB ALL cells (Boue & LeBien, 1988; Haso *et al.*, 2013; Kato *et al.*, 2013). Furthermore, it is known that αCD22 Abs are internalized upon binding to CD22 on the cell surface; therefore, it makes an excellent drug delivery vehicle (Hoelzer, 2013; Litzow, 2013; Sullivan-Chang *et al.*, 2013). As expected, our MXD3 siRNA-αCD22 Ab nanocomplexes did affect normal B cells, because B cells express both CD22 and MXD3. However, we expect that toxicities to B cells are acceptable side effects, given that anti-CD20, CD19 and CD22 antibodies, all of which target B cells, have been successfully used to treat leukaemias and lymphomas in the clinic (Thomas *et al.*, 2010; Kreitman & Pastan, 2011; Schindler *et al.*, 2011). It is also important to note that CD34+HSCs were spared from the cytotoxicity of the MXD3 siRNA-αCD22 Ab nanocomplexes. Therefore, normal B cells lost by the MXD3 siRNA-αCD22 Ab-nanocomplex treatment could be regenerated.

Lastly, SPIO NPs seem to be an efficient vehicle for siRNA delivery. As previous studies, including ours (data not shown), have shown that non-viral transfection of B cells, either malignant or normal, is extremely difficult, it is necessary to use a vehicle to deliver siRNA intracellularly. We chose SPIO NPs based on the reported advantages of the SPIO NPs: biocompatibility of iron oxide NPs, ability to modify the surface chemistry for efficient loading of siRNA based on electrostatic interactions, and the ease of separating bound molecules from the surface of the NPs using magnetic separation (Taratula *et al.*, 2011; Shah *et al.*, 2013; Duan *et al.*, 2014). In this study, we have demonstrated high efficiency (~100%) of loading siRNA molecules (271.6 moles per NP) based on electrostatic interactions between positively-charged NPs and negatively-charged siRNA molecules. We also demonstrated that both siRNA and antibody molecules were loaded on the surface of SPIO NPs based on physical interactions (Figure 1, Table I). The nanocomplexes, with or without αCD22 Abs, were efficiently delivered into both Reh cells and primary leukaemia cells (Figures 2A and B). We have shown a proof of concept that SPIO NPs can serve an as excellent vehicle for siRNA delivery. However, our results of control siRNA molecules with SPIO NPs indicated potential toxicity of the SPIO NPs (Figures 4, 5D and 6D). Toxicity was observed predominantly in primary cells, which was partly because the primary haematopoietic cells generally do not survive well *in vitro*. However, we speculate that the toxicity was due to the surface chemistry and net electrostatic charge on the surface of SPIO NPs, interactions of NPs with cell membranes and the intracellular fate of NPs. It is encouraging that SPIO NPs have been used successfully in clinical trials for imaging and therapeutic purposes (Tong *et al.*, 2011; de Rosales, 2014). Further studies are ongoing to modify the nanocomplexes and reduce their toxicities. These studies include covalent conjugation of siRNA and NPs and passivation of the surface with polyethylene glycol (PEG) molecules.

It is well known that monotherapy does not work for cancer; therefore, current treatments for preB ALL use combination chemotherapy. In this study, we demonstrated significant additive effects using a combination of one dose each of the MXD3 siRNA-αCD22 Ab nanocomplexes and either doxorubicin or vincristine at IC50 doses (Figure 7). The cytotoxicity of the MXD3 siRNA-αCD22 Ab nanocomplexes alone at 72 h after the treatments was enhanced by more than 20% when combined with vincristine (40.1% vs. 63.8%) or doxorubicin (40.1% vs. 61.2%). It is important to note that these additive effects were observed at a single treatment of each drug at IC50 dose. Therefore, it should be possible to find the most effective combination dose and schedule. Furthermore, we hypothesize that knockdown of MXD3 leads to activation of the apoptotic pathway in leukaemia cells, which sensitizes the cells to lower doses of chemotherapeutic agents, such as vincristine. This has the potential to improve efficacy and minimize systemic side effects. Therefore, we expect that our novel MXD3 siRNA-αCD22 Ab nanocomplexes have the potential to be a new addition to combination therapy for preB ALL and to lower the doses of current chemotherapy drugs, which will result in fewer side effects. It is also interesting to note that these additive effects were greatest when the drugs were added 4 h, rather than 24 h, after initial treatment with the siRNA-αCD22 Ab nanocomplexes, suggesting that siRNA nanocomplex treatment followed shortly by chemotherapy drug dosing may be the most effective timing for treatment of these cells *in vitro*. This may be due to the fast turn over time of MXD3. It is possible to further investigate the downstream pathway of MXD3 using combination therapies with other drugs with known mechanisms of action.

In summary, we have developed a new therapeutic concept using MXD3 siRNA-αCD22 Ab-SPIO NPs and demonstrated its potential as a novel therapy for preB ALL.

Acknowledgments

The authors thank Betty Ratliff, Jong Chung, Anjali Pawar and Jay Balagtas for assisting with primary sample collections, and Joyce Lee for obtaining drugs. This work was supported by the Hartwell Foundation (Satake) and National Center for Advancing Translational Sciences, National Institutes of Health, through grant #UL1 TR000002 (Satake).

References

August KJ, Narendran A, Neville KA. Pediatric relapsed or refractory leukemia: new pharmacotherapeutic developments and future directions. Drugs. 2013; 73:439–461. [PubMed: 23568274]

Barth M, Raetz E, Cairo MS. The future role of monoclonal antibody therapy in childhood acute leukaemias. British journal of haematology. 2012; 159:3–17. [PubMed: 22881237]

Boue DR, LeBien TW. Expression and structure of CD22 in acute leukemia. Blood. 1988; 71:1480–1486. [PubMed: 3258772]

Brown P. Treatment of infant leukemias: challenge and promise. Hematology / the Education Program of the American Society of Hematology. American Society of Hematology. Education Program. 2013; 2013:596–600. [PubMed: 24319237]

Daver N, O'Brien S. Novel therapeutic strategies in adult acute lymphoblastic leukemia--a focus on emerging monoclonal antibodies. Current hematologic malignancy reports. 2013; 8:123–131. [PubMed: 23539383]

de Rosales RT. Potential clinical applications of bimodal PET-MRI or SPECT-MRI agents. Journal of labelled compounds & radiopharmaceuticals. 2014

Doane TL, Chuang CH, Hill RJ, Burda C. Nanoparticle zeta -potentials. Accounts of chemical research. 2012; 45:317–326. [PubMed: 22074988]

Duan J, Dong J, Zhang T, Su Z, Ding J, Zhang Y, Mao X. Polyethyleneimine-functionalized iron oxide nanoparticles for systemic siRNA delivery in experimental arthritis. Nanomedicine. 2014; 9:789–801. [PubMed: 24392891]

Haso W, Lee DW, Shah NN, Stetler-Stevenson M, Yuan CM, Pastan IH, Dimitrov DS, Morgan RA, FitzGerald DJ, Barrett DM, Wayne AS, Mackall CL, Orentas RJ. Anti-CD22-chimeric antigen receptors targeting B-cell precursor acute lymphoblastic leukemia. Blood. 2013; 121:1165–1174. [PubMed: 23243285]

Hochhaus A, Kantarjian H. The development of dasatinib as a treatment for chronic myeloid leukemia (CML): from initial studies to application in newly diagnosed patients. Journal of cancer research and clinical oncology. 2013; 139:1971–1984. [PubMed: 23942795]

Hoelzer D. Targeted therapy with monoclonal antibodies in acute lymphoblastic leukemia. Current opinion in oncology. 2013; 25:701–706. [PubMed: 24097105]

Hothorn T, Zeileis A. Generalized maximally selected statistics. Biometrics. 2008; 64:1263–1269. [PubMed: 18325074]

Hothorn T, Bretz F, Westfall P. Simultaneous inference in general parametric models. Biometrical journal. Biometrische Zeitschrift. 2008; 50:346–363. [PubMed: 18481363]

Kato J, Satake N, O'Donnell RT, Abuhay M, Lewis C, Tuscano JM. Efficacy of a CD22-targeted antibody-saporin conjugate in a xenograft model of precursor-B cell acute lymphoblastic leukemia. Leukemia research. 2013; 37:83–88. [PubMed: 23040543]

Kreitman RJ, Pastan I. Antibody fusion proteins: anti-CD22 recombinant immunotoxin moxetumomab pasudotox. Clinical cancer research : an official journal of the American Association for Cancer Research. 2011; 17:6398–6405. [PubMed: 22003067]

Krishnan V, Rajasekaran AK. Clinical nanomedicine: a solution to the chemotherapy conundrum in pediatric leukemia therapy. Clinical pharmacology and therapeutics. 2014; 95:168–178. [PubMed: 24013811]

Kumar R, Kaur M, Silakari O. Physiological Modulation Approaches to Improve Cancer Chemotherapy: A Review. Anti-cancer agents in medicinal chemistry. 2013

Li J, Gupta S, Li C. Research perspectives: gold nanoparticles in cancer theranostics. Quantitative imaging in medicine and surgery. 2013; 3:284–291. [PubMed: 24404441]

Litzow MR. Monoclonal antibody-based therapies in the treatment of acute lymphoblastic leukemia. American Society of Clinical Oncology educational book / ASCO. American Society of Clinical Oncology. Meeting. 2013:294–299. [PubMed: 23714527]

Mullighan CG. Molecular genetics of B-precursor acute lymphoblastic leukemia. The Journal of clinical investigation. 2012; 122:3407–3415. [PubMed: 23023711]

Mussai F, Campana D, Bhojwani D, Stetler-Stevenson M, Steinberg SM, Wayne AS, Pastan I. Cytotoxicity of the anti-CD22 immunotoxin HA22 (CAT-8015) against paediatric acute lymphoblastic leukaemia. British journal of haematology. 2010; 150:352–358. [PubMed: 20528877]

Pui CH, Robison LL, Look AT. Acute lymphoblastic leukaemia. Lancet. 2008; 371:1030–1043. [PubMed: 18358930]

Ramsay AD, Rodriguez-Justo M. Chronic lymphocytic leukaemia--the role of the microenvironment pathogenesis and therapy. British journal of haematology. 2013; 162:15–24. [PubMed: 23617880]

Sanz MA, Iacoboni G, Montesinos P. Acute promyelocytic leukemia: do we have a new front-line standard of treatment? Current oncology reports. 2013; 15:445–449. [PubMed: 23990383]

Schindler J, Gajavelli S, Ravandi F, Shen Y, Parekh S, Braunchweig I, Barta S, Ghetie V, Vitetta E, Verma A. A phase I study of a combination of anti-CD19 and anti-CD22 immunotoxins (Combotox) in adult patients with refractory B-lineage acute lymphoblastic leukaemia. British journal of haematology. 2011; 154:471–476. [PubMed: 21732928]

Shah V, Taratula O, Garbuzenko OB, Patil ML, Savla R, Zhang M, Minko T. Genotoxicity of different nanocarriers: possible modifications for the delivery of nucleic acids. Current drug discovery technologies. 2013; 10:8–15. [PubMed: 22564170]

Sullivan-Chang L, O'Donnell RT, Tuscano JM. Targeting CD22 in B-cell malignancies: current status and clinical outlook. BioDrugs : clinical immunotherapeutics, biopharmaceuticals and gene therapy. 2013; 27:293–304.

Taratula O, Garbuzenko O, Savla R, Wang YA, He H, Minko T. Multifunctional nanomedicine platform for cancer specific delivery of siRNA by superparamagnetic iron oxide nanoparticles-dendrimer complexes. Current drug delivery. 2011; 8:59–69. [PubMed: 21034421]

Thomas DA, O'Brien S, Faderl S, Garcia-Manero G, Ferrajoli A, Wierda W, Ravandi F, Verstovsek S, Jorgensen JL, Bueso-Ramos C, Andreeff M, Pierce S, Garris R, Keating MJ, Cortes J, Kantarjian HM. Chemoimmunotherapy with a modified hyper-CVAD and rituximab regimen improves outcome in de novo Philadelphia chromosome-negative precursor B-lineage acute lymphoblastic leukemia. Journal of clinical oncology : official journal of the American Society of Clinical Oncology. 2010; 28:3880–3889. [PubMed: 20660823]

Tong L, Zhao M, Zhu S, Chen J. Synthesis and application of superparamagnetic iron oxide nanoparticles in targeted therapy and imaging of cancer. Frontiers of medicine. 2011; 5:379–387. [PubMed: 22198749]

van der Meel R, Vehmeijer LJ, Kok RJ, Storm G, van Gaal EV. Ligand-targeted particulate nanomedicines undergoing clinical evaluation: current status. Advanced drug delivery reviews. 2013; 65:1284–1298. [PubMed: 24018362]

Wiemels J. Perspectives on the causes of childhood leukemia. Chemico-biological interactions. 2012; 196:59–67. [PubMed: 22326931]

Zerra P, Cochran TR, Franco VI, Lipshultz SE. An expert opinion on pharmacologic approaches to reducing the cardiotoxicity of childhood acute lymphoblastic leukemia therapies. Expert opinion on pharmacotherapy. 2013; 14:1497–1513. [PubMed: 23705955]

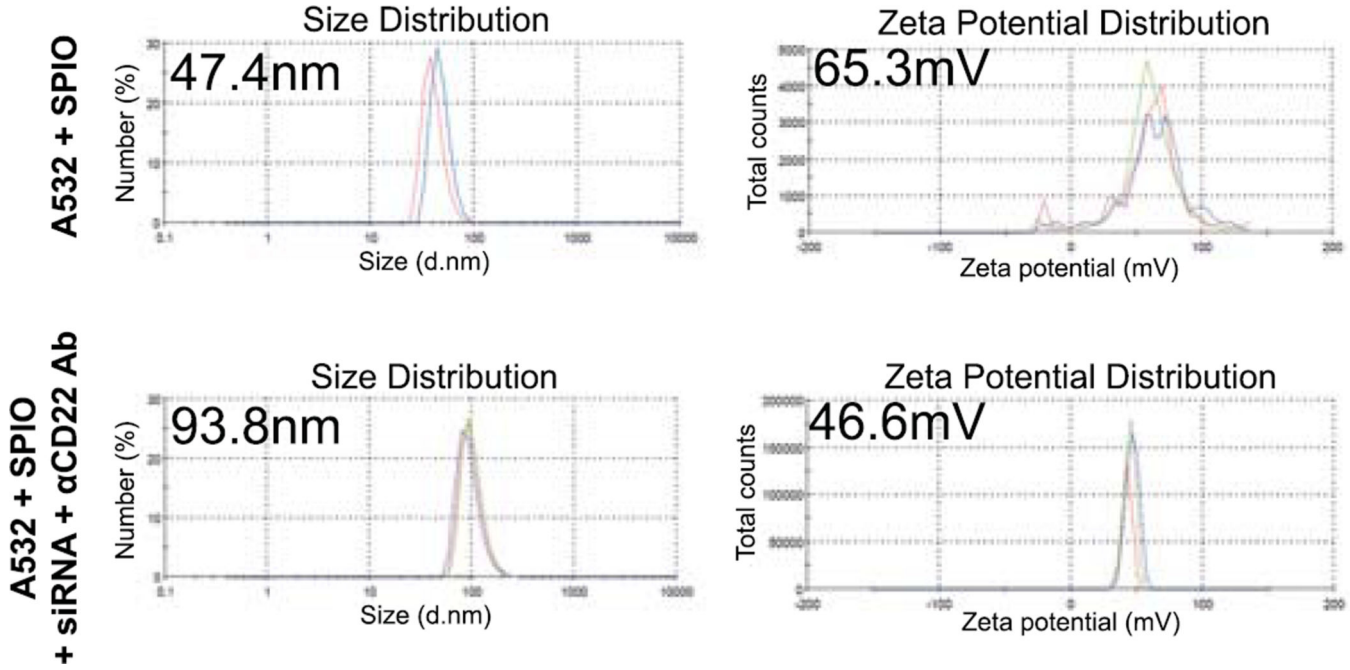

Figure 1. Nanocomplexes are created with siRNAs, αCD22 Abs, and SPIO NPs

Diameter and zeta potential of the siRNA-αCD22 Ab-nanocomplexes. A532-labelled SPIO NPs were combined with siRNAs and αCD22 Abs. The size and zeta potential of the nanocomplexes changed after combining the siRNAs and αCD22 Abs. Average diameter or zeta potential of SPIO NPs + A532 and SPIO NPs + A532 + siRNA + CD22 is indicated in the left upper corner of each graph.

A532, Alexa Fluor 532; αCD22 Ab, anti-CD22 antibody; SPIO, superparamagnetic iron oxide; NP, nanoparticle; siRNA, small interfering RNA.

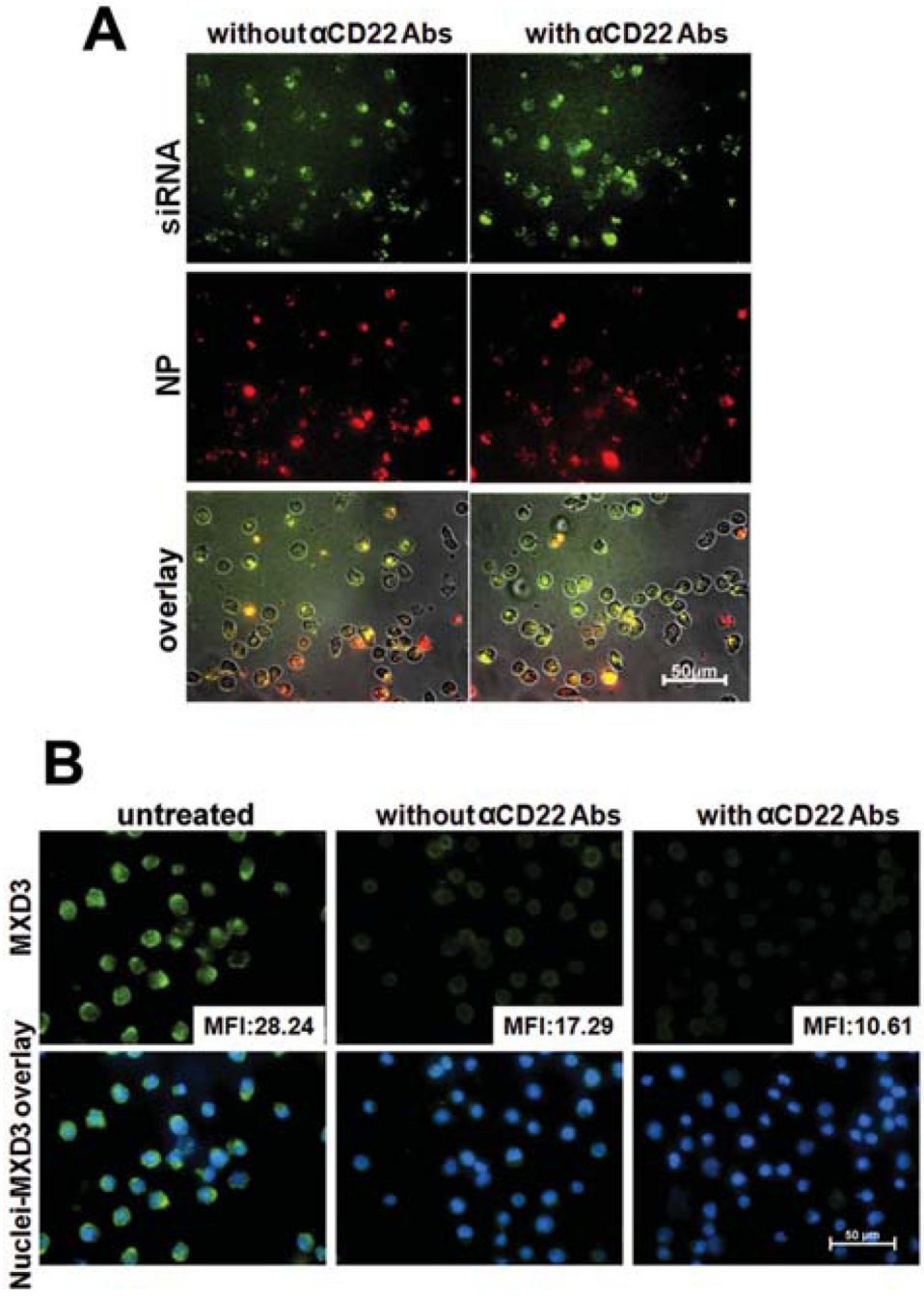

Figure 2. Efficient delivery of siRNA-αCD22 Ab-SPIO NPs and MXD3 knockdown in preB ALL cells

(A) Intracellular uptake of the siRNA-αCD22 Ab-SPIO NPs with A488-labelled siRNAs, FITC-labelled αCD22 Abs and A532-labelled SPIO NPs to Reh cells. More nanocomplexes were observed in the cells treated with the nanocomplexes with αCD22 Abs than those without Abs. The images were taken 4 h after treatments.

(B) Addition of αCD22 Abs to the siRNA-αCD22 Ab-SPIO NPs enhancing the efficiency of MXD3 knockdown in Reh cells. Reh cells treated with the nanocomplexes, with or

without αCD22 Abs, or left untreated as control, were measured for MXD3 protein expression 4 h after treatments. For each image, the protein level was measured by mean fluorescence intensity (MFI) in each cell in the field and averaged MFI is shown in the right lower corner of each MXD3 image.

αCD22 Ab, anti-CD22 antibody; SPIO, superparamagnetic iron oxide; NP, nanoparticle; siRNA, small interfering RNA.

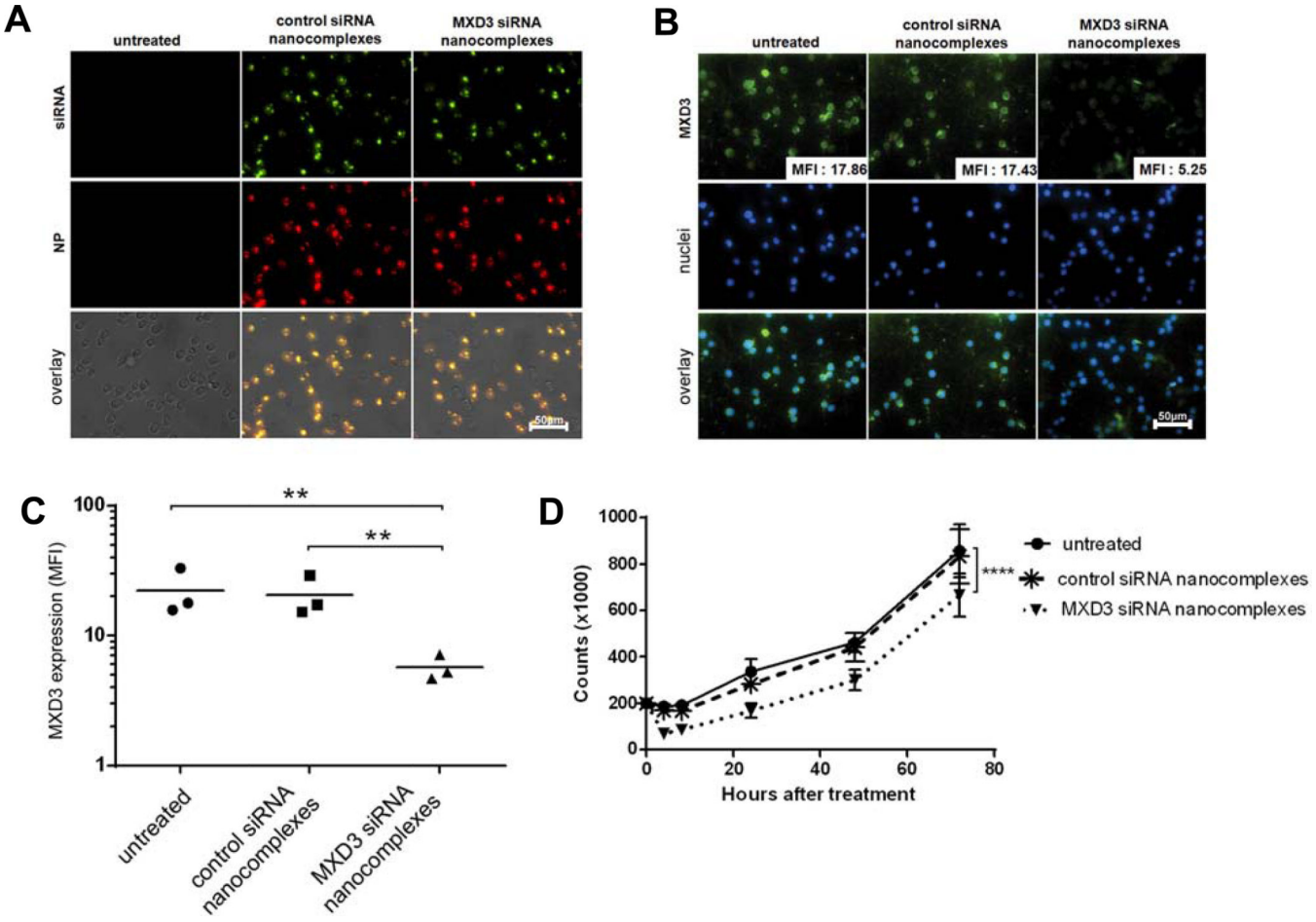

Figure 3. Intracellular delivery of the MXD3 siRNA-αCD22 Ab-SPIO NPs results in MXD3 knockdown and cell growth inhibition in Reh cells *in vitro*

(A) Intracellular delivery of the siRNA-αCD22 Ab-SPIO NPs. The siRNA-αCD22 Ab-SPIO NPs are composed of A488-labelled control or MXD3 siRNAs, FITC-labelled αCD22 Abs, and A532-labelled SPIO NPs. The images were taken 4 hours after treatment with siRNA-αCD22 Ab-SPIO NPs. Untreated cells were shown as a control.

(B) MXD3 knockdown in the cells treated with the MXD3 siRNA-αCD22 Ab-SPIO NPs at 4 hours after treatment. Reh cells that were treated with the control siRNA-αCD22 Ab-SPIO NPs did not exhibit the same level of MXD3 knockdown and showed similar levels of expression to untreated cells. For each image, protein level was measured by MFI in each cell in the field and the average MFI is shown in the right lower corner of each MXD3 image.

(C) MXD3 protein knockdown quantified using MFI. The cells treated with MXD3 siRNA-αCD22 Ab-SPIO NPs showed decreased MXD3 protein expression compared with the cells treated with the control siRNA-αCD22 Ab-SPIO NPs or untreated cells. Each point represents the average MFI of all measured cells per treatment type, in 3 independent experiments. Untreated vs. MXD3 siRNA-αCD22 Ab-SPIO NPs (**) $p = 0.00606$, control vs. MXD3 siRNA-αCD22 Ab-SPIO NPs (**) $p = 0.00814$. The p-values are from the post-hoc Tukey studenized range test on a one-way ANOVA of log(MFI).

(D) Reduced cell growth in the cells treated with the MXD3 siRNA-αCD22 Ab-SPIO NPs. Data points indicate mean values of independent cell count in triplicates from 3 independent experiments. Live cell count was measured at 4, 8, 24, 48 and 72 h after a single treatment with the MXD3 or control siRNA-αCD22 Ab-SPIO NPs. Untreated cells were also used as a control. Error bars represent range (n=9 for each time point). The cells treated with the MXD3 siRNA-αCD22 Ab-SPIO NPs had significantly fewer live cells than either the untreated cells or the cells treated with the control siRNA-αCD22 Ab-SPIO NPs ($p < 0.0001$).

αCD22 Ab, anti-CD22 antibody; SPIO, superparamagnetic iron oxide; NP, nanoparticle; siRNA, small interfering RNA; MFI, mean fluorescence intensity.

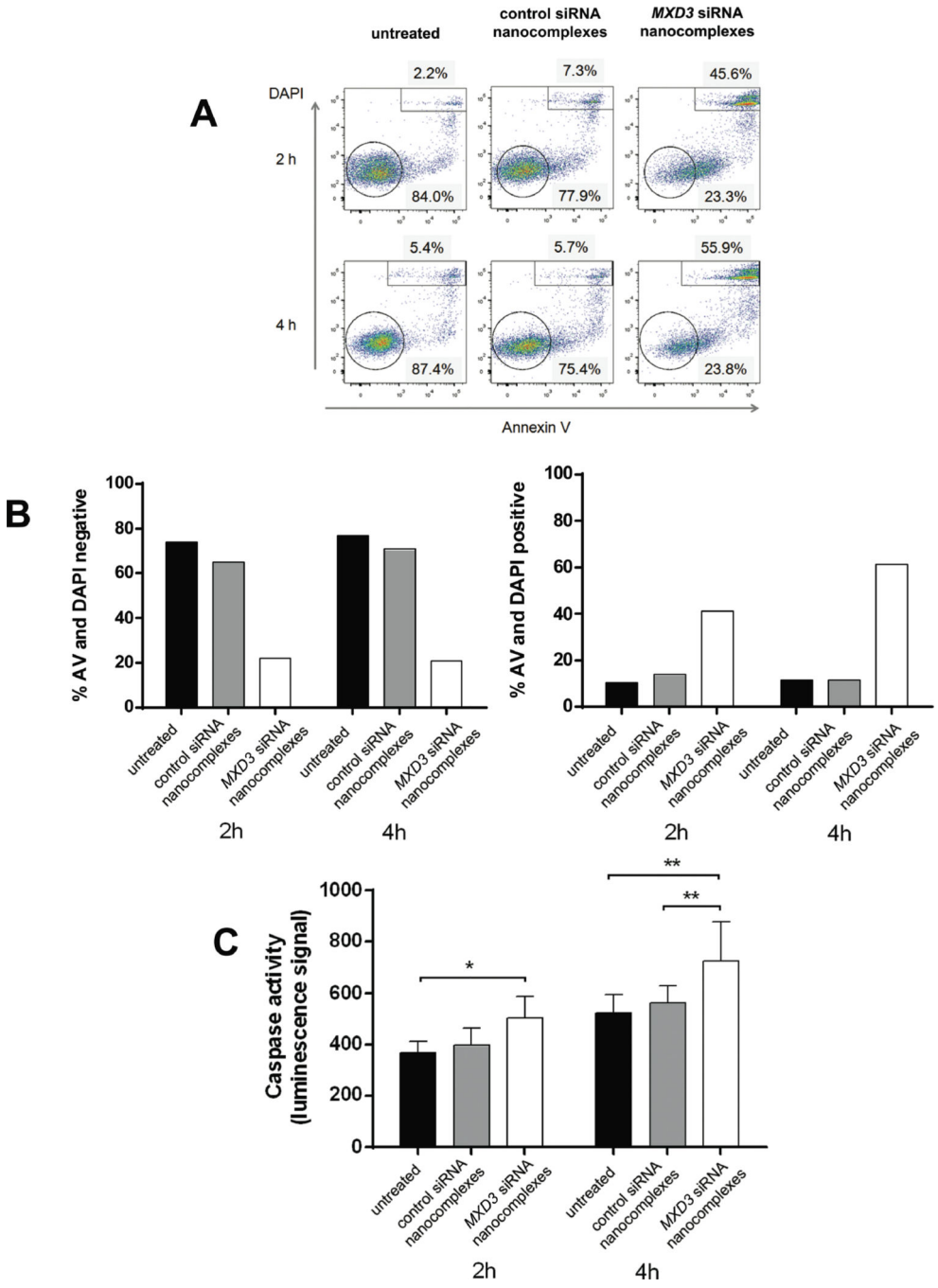

Figure 4. Treatment of Reh cells with the MXD3 siRNA-αCD22 Ab-SPIO NPs increases apoptosis

(A and B) Cell death measured by annexin V and DAPI. (A) Reh cells treated with the MXD3 siRNA-αCD22 Ab-SPIO NPs had fewer live cells (negative for annexin V and DAPI) and more dead cells (positive for annexin V and DAPI) than untreated cells or cells treated with the control siRNA-αCD22 Ab-SPIO NPs at 2 and 4 h after treatment. The circled or rectangle events indicate double negative or double positive cells, respectively. Graphs show one representative experiment (from a total of 2 experiments repeated).

(B) Flow cytometry results at 2 and 4 h from 2 experiments. Data as mean (n = 2 for each time point). The MXD3 siRNA nanocomplex-treated cells showed significantly fewer double negative cells and significantly more double positive cells at both time points: double negative (vs. untreated $p = 0.0000154$, vs. control $p = 0.0000484$) and double positive (vs. untreated $p = 0.0006531$, vs. control $p = 0.0008478$). This analysis used a three-way ANOVA with Treatment, Time and Experiment Number as factors. The p-values are from the post-hoc Tukey studentized range test.

(C) Cell death measured by caspase 3 and 7 activities. Cells were treated the same way as in (A) with the same control. Histograms represent caspase activity measured by luminescence signal at 2 and 4 hours after treatment. Data include 2 independent experiments. Data as mean ± SD. (n = 9 for each time point). We used a two-way ANOVA on Treatment and Time, with post-hoc comparisons from the Tukey studentized range test. The cells treated with the MXD3 siRNA nanocomplexes had a significantly higher average caspase 3 and 7 activity levels than either the untreated cells ($p = 0.0127$) or those treated with the control siRNA nanocomplexes ($p = 0.0380$)

αCD22 Ab, anti-CD22 antibody; SPIO, superparamagnetic iron oxide; NP, nanoparticle; siRNA, small interfering RNA; AV, Annexin V; DAPI, 4',6-diamidino-2-phenylindole.

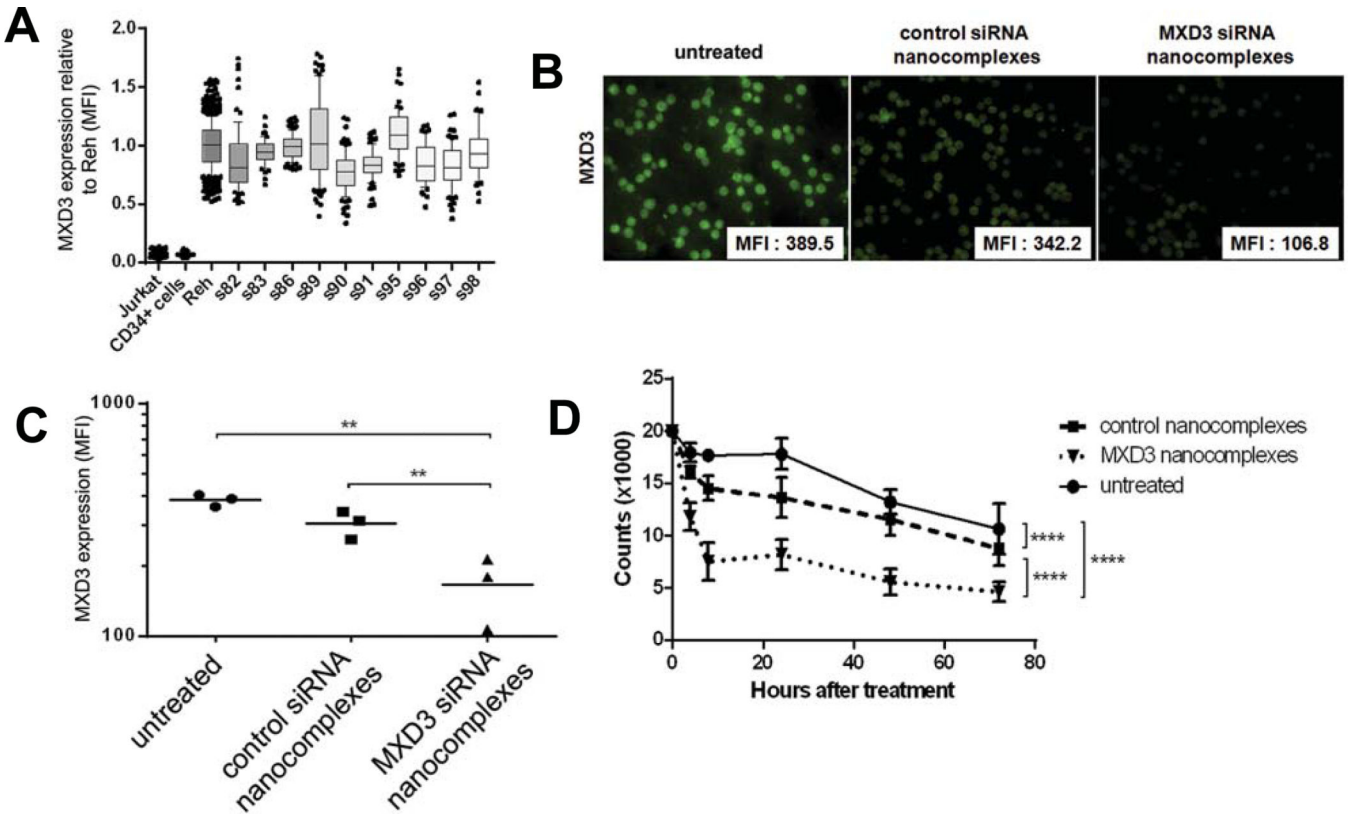

Figure 5. MXD3 siRNA-αCD22 Ab-SPIO NP treatment results in MXD3 knockdown and decreased viability of primary preB ALL cells *in vitro*

(A) High MXD3 protein expression in a series of primary preB ALL samples. Ten primary preB ALL samples showed high MXD3 protein expression relative to Reh cells. Jurkat cells and normal CD34+HSCs showed low expression. Boxes represent MXD3 protein levels in individual cells relative to those in Reh cells, measured by MFI. Bars indicate mean and whiskers 10–90 percentile represented as individually plotted points.

(B) MXD3 knockdown in a primary leukaemia sample treated with the MXD3 siRNA-αCD22 Ab-SPIO NPs at 4 h after treatment. Cells that were treated with the control siRNA-αCD22 Ab-SPIO NPs did not exhibit the same level of MXD3 knockdown. For each image, protein level was measured by MFI in each cell in the field and the average MFI is shown in the right lower corner of each MXD3 image.

(C) The MXD3 protein level measured by MFI. The cells treated with MXD3 siRNA-αCD22 Ab-SPIO NPs showed significantly decreased MXD3 protein expression compared with the cells treated with the control siRNA-αCD22 Ab-SPIO NPs or untreated cells. Each point represents the average MFI of all measured cells per treatment type, in 3 independent experiments. Untreated vs. MXD3 siRNA-αCD22 Ab-SPIO NPs (**) $p = 0.00735$, control vs. MXD3 siRNA-αCD22 Ab-SPIO NPs (*) $p = 0.03108$

(D) Accelerated cell death in the primary leukaemia cells treated with the MXD3 siRNA-αCD22 Ab-SPIO NPs. Data points indicate mean values of independent cell count in triplicates from 3 independent experiments. Live cell count was measured at 4, 8, 24, 48 and 72 h after single treatment with the MXD3 or control siRNA-αCD22 Ab-SPIO NPs. Untreated cells were also used as a control. Data as mean ± SD. Untreated vs. MXD3

siRNA-αCD22 Ab-SPIO NPs (****) p< 0.00001, untreated vs. control siRNA-αCD22 Ab-SPIO NPs (****) p = 0.000035, control vs. MXD3 siRNA-αCD22 Ab-SPIO NPs (****) p < 0.00001.

αCD22 Ab, anti-CD22 antibody; SPIO, superparamagnetic iron oxide; NP, nanoparticle; siRNA, small interfering RNA; MFI, mean fluorescence intensity; SD, standard deviation.

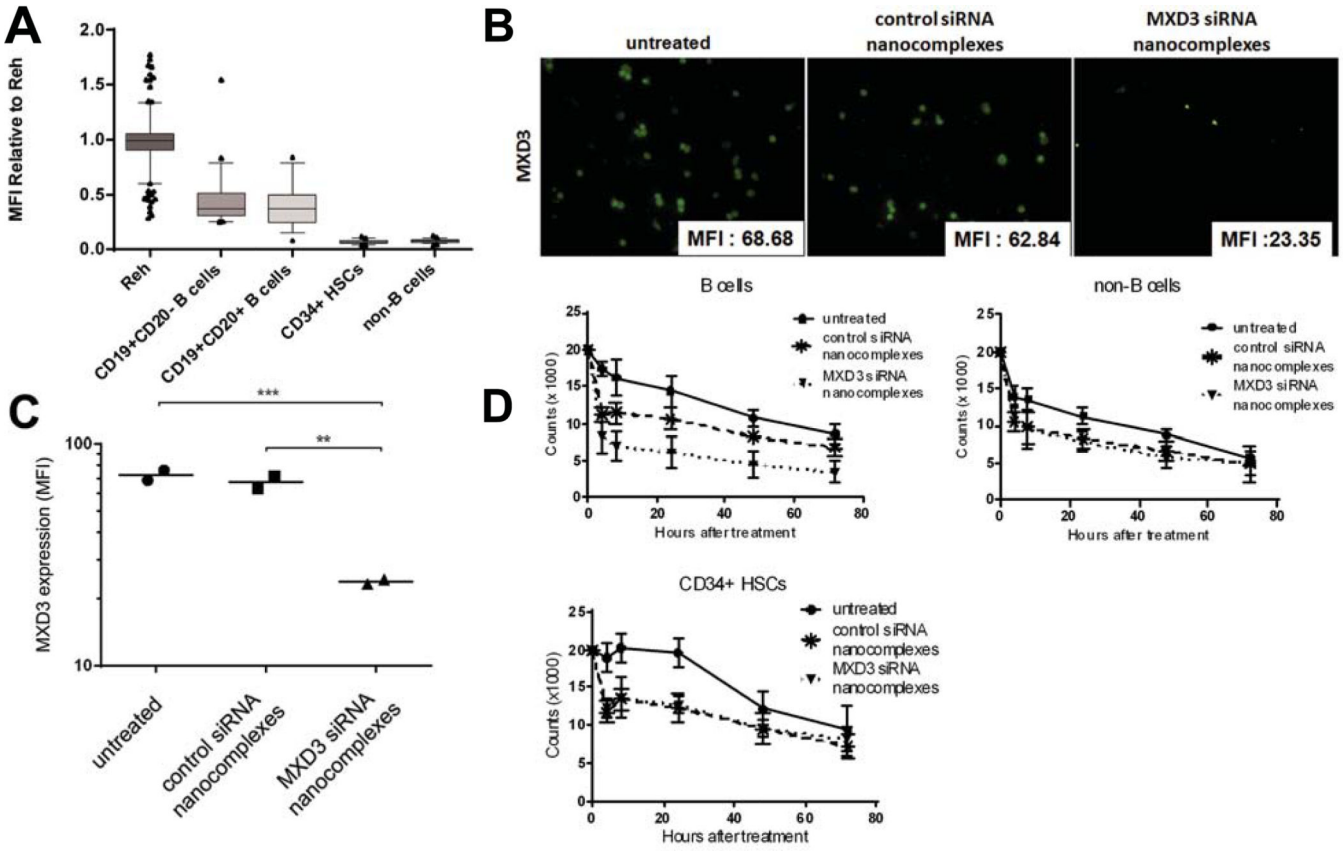

Figure 6. Primary normal B cells, but not CD34+HSCs, express some MXD3, and the MXD3 siRNA-αCD22 Ab-SPIO NP treatment results in MXD3 knockdown and accelerated cell death *in vitro*

(A) Some MXD3 protein expression was observed in B cells, but not in CD34+HSCs. Both mature and immature B cells showed less than 50% MXD3 protein expression compared to Reh cells, but CD34+HSCs and non-B cells showed minimal MXD3 expression. Boxes represent MXD3 protein levels in individual cells relative to those in Reh cells, measured by MFI. Bars indicate mean and whiskers, 10–90 percentile represented as individually plotted points.

(B) MXD3 knockdown in the normal B cells treated with the MXD3 siRNA-αCD22 Ab-SPIO NPs at 4 h after treatment. Cells that were treated with the control siRNA-αCD22 Ab-SPIO NPs did not exhibit the same level of MXD3 knockdown. For each image, the protein level was measured by MFI in each cell in the field and the average MFI is shown in the right lower corner of each MXD3 image.

(C) MXD3 protein level measured by MFI. The cells treated with MXD3 siRNA-αCD22 Ab-SPIO NPs showed significantly decreased MXD3 protein expression compared with the cells treated with the control siRNA-αCD22 Ab-SPIO NPs or untreated cells. Each point represents the average MFI of all measured cells per treatment type in triplicates in 2 independent experiments. The MXD3 protein expression was significantly lower in the cells treated with MXD3 siRNA-αCD22 Ab-SPIO NPs than in untreated cells ($p = 0.0012$) and in cells treated with the control siRNA-αCD22 Ab-SPIO NPs ($p = 0.0015$) using the Tukey studentized range test in an ANOVA on log(MFI).

(D) Accelerated cell death in the B cells treated with the MXD3 siRNA-αCD22 Ab-SPIO NPs. Data points indicate mean values of independent cell count in triplicates from 2 independent experiments. Live cell count was measured at 4, 8, 24, 48 and 72 h after single treatment with the MXD3 or control siRNA-αCD22 Ab-SPIO NPs. Untreated cells were also used as a control. Data as mean ± SD. For all three cell types, the control and MXD3 siRNA-αCD22 Ab-SPIO NPs differ significantly from the untreated ($p < 0.0002$ for each of the six comparisons). The MXD3 and control siRNA-αCD22 Ab-SPIO NP treated groups differ significantly in B cell count ($p = 0.00003$), but not in CD34+HSCs ($p = 0.91$) or non-B cells ($p = 0.96$). This analysis used a three-way ANOVA with Treatment, Time, and Experiment Number as factors. The p-values are from the post-hoc Tukey studentized range test.

αCD22 Ab, anti-CD22 antibody; SPIO, superparamagnetic iron oxide; NP, nanoparticle; siRNA, small interfering RNA; MFI, mean fluorescence intensity; SD, standard deviation.

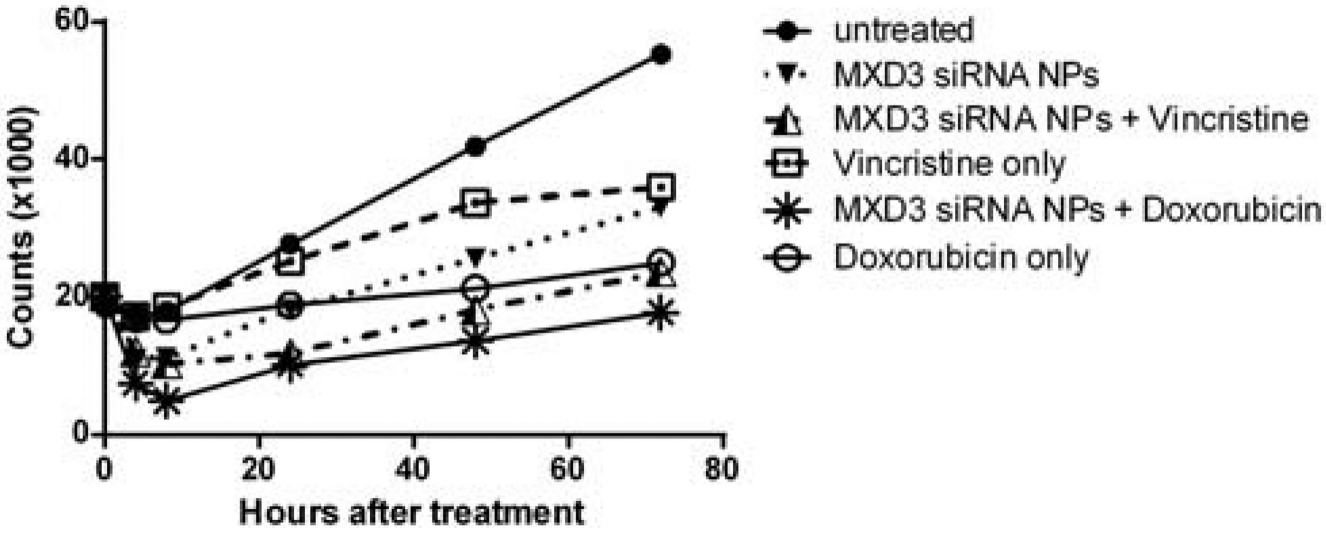

Figure 7. Doxorubicin or vincristine enhanced the treatment effects of the MXD3 siRNA-αCD22 Ab-SPIO NPs in Reh cells *in vitro*

Combination single treatment of the MXD3 siRNA-αCD22 Ab-SPIO NPs and doxorubicin or vincristine at the 50% inhibitory concentration (IC50) doses showed significantly enhanced cytotoxicity in Reh cells. Data were collected in triplicates, with 2 independent experiments (n = 6). Data as mean. MXD3 siRNA-αCD22 Ab-SPIO NPs only vs. MXD3 siRNA-αCD22 Ab-SPIO NPs + doxorubicin (****) $p < 0.0000001$, doxorubicin only vs. MXD3 siRNA-αCD22 Ab-SPIO NPs + doxorubicin (****) $p = 0.0000032$, MXD3 siRNA-αCD22 Ab-SPIO NPs only vs. MXD3 siRNA-αCD22 Ab-SPIO NPs + vincristine (****) $p < 0.0001$ and vincristine only vs. MXD3 siRNA-αCD22 Ab-SPIO NPs + vincristine (****) $p < 0.0000001$.

SPIO, superparamagnetic iron oxide; NP, nanoparticle; siRNA, small interfering RNA.

Table I

Efficiency of siRNA and αCD22 antibody loading onto SPIO nanoparticles

APC		
	Absorbance	**% Intensity**
αCD22 Ab-SPIO pellet	1.20E+06	89.9
supernatant (unbound αCD22 Ab)	1.35E+05	10.1
siRNA-αCD22 Ab-SPIO pellet	6.89E+05	47.1
supernatant (unbound αCD22 Ab)	7.74E+05	52.9
Alexa488		
	Absorbance	% Intensity
siRNA-SPIO pellet	6.06E+07	95.3
supernatant (unbound siRNA)	2.96E+06	4.66
siRNA-αCD22 Ab-SPIO pellet	5.58E+07	100
supernatant (unbound siRNA)	1.27E+03	0

APC, allophycocyanin; Alexa488, Alexa Fluor 488; αCD22 Ab, anti-CD22 antibody; SPIO, superparamagnetic iron oxide; siRNA, small interfering RNA.